EFFECTS OF PLASMA SHAPE AND PROFILES ON EDGE STABILITY IN DIII–D

L.L. LAO, J.R. FERRON, R.L. MILLER, T.H. OSBORNE, V.S. CHAN, R.J. GROEBNER,
G.L. JACKSON, R.J. LA HAYE, E.J. STRAIT, T.S.TAYLOR, A.D. TURNBULL
DIII–D National Fusion Facility, General Atomics, San Diego, California, U.S.A.

E.J. DOYLE
University of California, Los Angeles, California, U.S.A.

E.A. LAZARUS, M. MURAKAMI
Oak Ridge National Laboratory, Oak Ridge, Tennessee, U.S.A.

G.R. MCKEE
University of Wisconsin, Madison, Wisconsin, U.S.A.

B.W. RICE
Lawrence Livermore National Laboratory, Livermore, California, U.S.A.

C. ZHANG, L. CHEN
Institute of Plasma Physics, Chinese Academy of Science, Hefei, P.R. China

Abstract

The results of recent experimental and theoretical studies concerning the effects of plasma shape and current and pressure profiles on edge instabilities in DIII–D are presented. Magnetic oscillations with toroidal mode number $n \approx 2$–9 and a fast growth time $\gamma^{-1} = 20$-150 μs are often observed prior to the first giant type I ELM in discharges with moderate squareness. High n ideal ballooning second stability access encourages edge instabilities by facilitating the buildup of the edge pressure gradient and bootstrap current density which destabilize the intermediate to low n modes. Analysis suggests that discharges with large edge pressure gradient and bootstrap current density are more unstable to $n > 1$ modes. Calculations and experimental results show that ELM amplitude and frequency can be varied by controlling access to the second ballooning stability regime at the edge through variation of the squareness of the discharge shape. A new method is proposed to control edge instabilities by reducing access to the second ballooning stability regime at the edge using high order local perturbation of the plasma shape in the outboard bad curvature region.

1. INTRODUCTION AND OVERVIEW

One of the major goals of advanced tokamak research is to develop plasma configurations with good confinement and improved stability at high β. In DIII–D, high performance discharges with a high confinement edge and various plasma shapes and current profiles have been produced. All these discharges exhibit enhanced confinement in the plasma edge region, leading to a large edge pressure gradient P′ and bootstrap current density J_{BS}. These edge conditions typically drive edge instabilities which terminate the discharge high performance phase, often accompanied by a permanent loss of the discharge internal transport barrier. An improved understanding of these edge instabilities is essential to optimize and sustain the discharge performance. Furthermore, the performance of future tokamak devices such as ITER is sensitive to the magnitude of the edge pressure pedestal, which is limited by edge instabilities. An improved understanding of the edge instabilities will also provide a more accurate prediction of the performance of future tokamak devices.

Edge instabilities often appear as cycles of edge localized mode (ELM) [1,2] with varying amplitude and frequency depending on the edge conditions, the power loss from the core, and the plasma shape. The effect of ELMs on the discharge performance varies with the ELM amplitude and frequency. An ELM of large amplitude can substantially degrade the plasma performance and result in large energy flux to the divertor. One of the major issues facing advanced tokamak research is the

control of edge P' and J_{BS} which drive these instabilities. In this paper, the results of recent experimental and theoretical studies concerning the effects of plasma shape and current and pressure profiles on edge instabilities in DIII–D are presented. Here, we explore the use of plasma shape as a means to control the edge P' and J_{BS}, as well as a means to improve our understanding of these instabilities. Since these instabilities are sensitive to details of edge P' and J_{BS}, most of the studies make use of the recently upgraded 35-channel Motional Stark Effect (MSE) current profile diagnostic [3] and recent improvements to our equilibrium and stability analysis tools to allow a more definite comparison with theory.

In DIII–D discharges with moderate squareness, prior to the first giant type I ELM, magnetic oscillations with toroidal mode number $n \approx$ 2–9 and a fast growth time $\gamma^{-1} =$ 20–150 µs are often observed. Ideal stability calculations using simulated and experimental equilibria are in general consistent with various observed features of these instabilities. High n ballooning stability results show that the edge region of these discharges is in the second ballooning stability regime, and that the edge P' substantially exceeds the first ballooning stability limit [4]. Low n stability results show that discharges with large edge P' and current density J are more unstable to $n > 1$ modes [5–7]. These results indicate that edge instabilities may be the outcome of a complex interaction among the high n ballooning modes, the low n kink/ballooning/peeling modes and the edge P' and J. The results also suggest that the large edge P' and J may be controlled by reducing the ballooning second stability access in the edge, thereby providing a means to control edge instabilities. Indeed, calculations and experimental results show that ELM amplitude and frequency can be varied by controlling access to the ballooning second stability regime at the edge through variation of the squareness of the discharge shape [8–10]. Motivated by these results from the squareness experiments, recent calculations show that a high order local perturbation of the plasma shape in the outboard bad curvature region can also reduce and eliminate second ballooning stability access in the plasma edge region. Since the perturbation is local, these configurations tend to retain many of the favorable low n stability property of Dee-shaped plasmas.

In Section 2, the general features of edge instabilities are introduced together with a discussion of magnetic fluctuations. The role of edge P' and current density J on high n ballooning and moderate n kink/ballooning/ peeling modes is discussed in Section 3. This is followed by a discussion of the effects of plasma shaping on ELMs in Section 4. A discussion and a summary is given in Section 5.

2. EDGE INSTABILITIES AND MAGNETIC FLUCTUATIONS

The performance of DIII–D discharges with a high confinement edge is typically limited by edge instabilities. This is illustrated in Fig. 1, where the time evolution of an H–mode discharge is shown. This discharge carries a plasma current I_P of 1.9 MA and has a vacuum toroidal magnetic field B_T of 2.1 T at the vacuum vessel center. To produce a negative central magnetic shear, up to 14.5 MW of neutral beam power P_B is injected into the plasma during the current ramp up phase. The discharge makes a transition into the H–mode phase at 1.58 s, as can be seen by the rapid increase in the edge electron temperature T_e near $\rho \approx 0.9$ shown in Fig. 1(b). The normalized toroidal beta β_N increases to 2.5 and remains at that value as P_B is reduced from 14.5 MW to 12.1 MW. At 1.876 s, a giant type I ELM occurs as shown by the spikes in the divertor D_α radiation and the outboard mid-plane Mirnov signal given in Figs. 1(b) and 1(c), respectively. The giant ELM causes a rapid drop of the edge T_e and a decrease in the global β_N. As subsequent ELMs occur , the edge T_e and β_N continue to decrease. The magnetic oscillation which initiates the giant type I ELM has a toroidal mode number $n \approx 5$ and a fast growth time $\gamma^{-1} \approx 150$ µs.

These type I ELMs and edge instabilities have been observed in DIII–D H– and VH–mode discharges with various poloidal cross sections including single- and double-null divertors, Dee and crescent shapes. Prior to the first giant type I ELM, magnetic oscillations with toroidal mode number $n \approx$ 2-9 are often observed. This is illustrated in Fig. 2. All these discharges have broad pressure profiles and moderate amount of squareness in the plasma shape. The magnetic precursors are localized poloidally in the bad curvature region as well as toroidally with a fast growth time $\gamma^{-1} =$ 20–150 µs [5,11]. They usually rotate in the electron diamagnetic drift direction, which is consistent with a location near the plasma edge where the $E \times B$ drift is dominated by the diamagnetic drift associated with the large edge P'. They have been observed in discharges with various current profiles and over a wide range of $\beta_N =$ 2.0–5.0. The attainable beta values decrease with the fraction of plasma current contained in the edge region [7] and are consistent with the previously observed operational beta limit of $\beta_N \approx 4 \, l_i$ [12,13]. As shown in Figs. 2 (a–c), the instabilities can have global effects, ranging from a
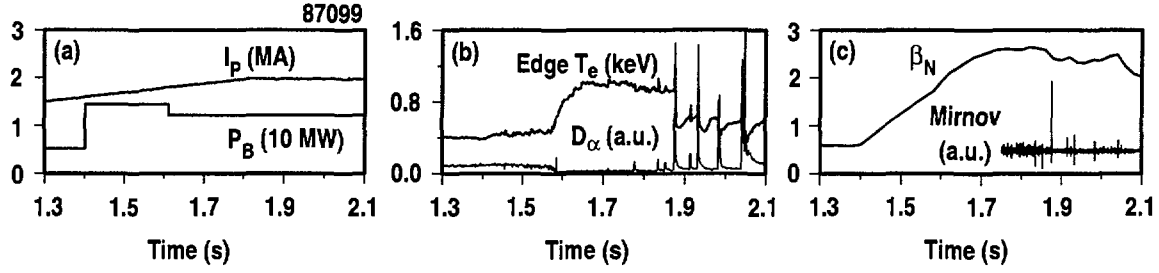
FIG. 1. *Time evolution of DIII–D H–mode discharge 87099. (a) Plasma current and injected neutral beam power; (b) edge electron temperature near $\rho \approx 0.9$ and divertor D_α radiation; (c) normalized toroidal beta and Mirnov oscillation in the outboard midplane region.*
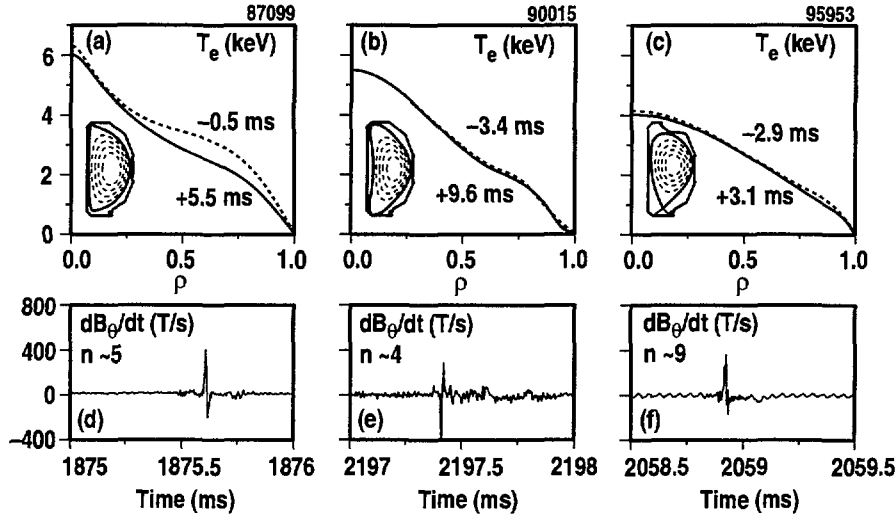

FIG. 2 *Magnetic precursors and radial electron temperature profiles before (dashed) and after (solid) an edge instability for (a) a double-null divertor discharge, (b) a crescent-shaped discharge, and (c) a lower single-null divertor discharge.*

slight decrease of edge T_e with a saturation of β_N, to a drop of T_e across the entire plasma with a decrease in β_N. The transport barriers observed in VH–mode and negative central magnetic shear discharges are usually destroyed. These moderate to low n edge instabilities have many features similar to the outer modes observed in the hot-ion H–mode in JET [14]. However, the outer modes observed in JET generally have $n = 1$, whereas in DIII–D modes with $n = 2$–9 are observed. After this first giant ELM, the discharge usually evolves into a quasi-stationary phase at similar or lower β_N values. The low to moderate $n = 2$–9 magnetic perturbations are rarely observed during this phase. Modes with $n > 9$ are difficult to resolve with the existing DIII–D magnetic probes, which suggests that these later ELMs may be driven by edge instabilities with significantly higher n.

Localized reflectometer measurements of density fluctuations at the outboard mid-plane show that the magnetic precursors coincide with, or in some cases are preceded by, bursts of increased density perturbation localized to the plasma edge. In cases where a radial propagation can be discerned, the perturbation initiates in the high pressure gradient edge region, and propagates outward into the scrape-off layer.

3. ROLE OF P′ AND J IN HIGH n BALLOONING AND MODERATE n MODES

High n ballooning stability analyses show that prior to the onset of the edge instabilities the discharges often have access to the second ballooning stability regime in the outer edge region and the edge P′ substantially exceeds the first ballooning stability limit. This is illustrated in Fig. 3 for a double-null and a lower single-null divertor discharge. The equilibria used in the stability analysis are fully reconstructed from equilibrium analysis using external magnetic data, MSE data, kinetic profile data, and the EFIT code [15]. Stability to the high n ballooning modes is evaluated using the BALOO
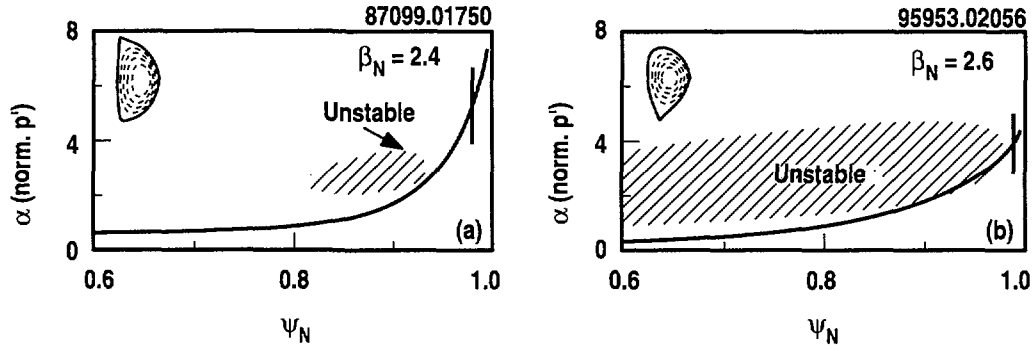
FIG. 3. Ideal ballooning stability of two DIII–D H–mode discharges 87099 at 1750 ms and 95953 at 2056 ms showing the edge regions have second ballooning stability access.

code [16], which now employs a local equilibrium representation [17]. As shown in Figs. 3(a) and 3(b), the double-null divertor discharge, which has a $n \approx 5$ magnetic precursor prior to the first giant ELM [Fig. 2(a)], has a much larger edge P' and a much wider edge second ballooning regime access than the lower single-null divertor discharge which has a $n \approx 9$ magnetic precursor [Fig. 2(c)]. Access to the second ballooning stability regime in the outer edge is necessary to allow buildup of a large edge P' often observed in the DIII–D H– and VH–mode discharges. The radial extent of the region with second ballooning stability access depends on the plasma shape and the edge J. An increase in the edge J_{BS} due to an increase in the edge P' will lead to a further opening of the second ballooning stability zone, in turn allowing a further increase in the edge P' and J_{BS}. Similar results on ballooning stability have also been reported in Ref. 18. The effects of the plasma shaping on the ballooning stability will be discussed in the next section.

Results of low n stability analyses using simulated and experimental equilibria are consistent with various observed features of the experiments and show that equilibria with broad pressure profiles and large edge P' and J are more unstable to modes with $n > 1$. This is illustrated in Fig. 4 for a sequence of simulated equilibria based on the experimental discharge shown in Fig. 1 but with a simpler pressure gradient profile that has the shape of a step function [Fig. 4(a)]. The stability to the ideal n = 1–3 modes is evaluated using the GATO code [19] with a conducting wall at the surrounding vacuum vessel. As the radial width of the large edge P' region $\delta\Psi$p' is increased, the n = 3 modes become unstable first. These unstable modes are kink/ballooning modes with a large peeling component. With a further increase in $\delta\Psi$p', the $n = 2$ modes then become unstable. As shown in Fig. 4(c), the radial structure of the unstable modes exhibits a large peeling component in the edge. As expected, the external radial width of the unstable modes $\delta\Psi$mode increases with $\delta\Psi$p'. The $n = 1$ modes are stable in all cases. These low n =2,3 modes are driven by both the edge P' and J [5,6].
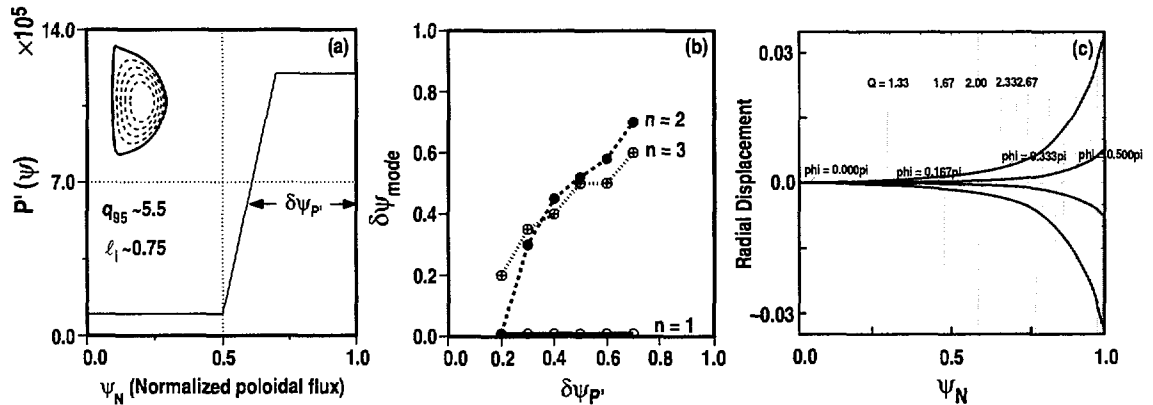

FIG. 4. (a) Equilibrium flux surface and radial profile of pressure gradient used in the low n stability analysis, (b) variation of external radial width of unstable modes with the width of the large edge P' region, (c) radial structure of a n=3 unstable mode.

4. EFFECTS OF PLASMA SHAPING ON ELMS

The effects of plasma shaping on edge instabilities and ELMs are considered in this section. Theoretical calculations suggest that second ballooning stability access in the outer edge region is reduced at low and high squareness [8]. This is illustrated in Fig. 5, where the edge current density (normalized to the collisionless bootstrap current at the edge) required to gain second stability access in the plasma edge as a function of the squareness of the plasma shape is shown. With $C_{boot} = (J/J_{BS})|_{edge} = 1$ the current density needed to gain access is the bootstrap current density based on the collisionless model [20], with $C_{boot} = 0$ no current density is required. As shown in Fig. 5, at low and high squareness C_{boot} becomes greater than 1 suggesting that second ballooning stability access is more difficult at these squareness values. The calculations are done using self-consistent pressure and bootstrap current density profiles. This reduction of second ballooning stability access is due to the increased weighting of the magnetic field lines in the outboard bad curvature region at high or low squareness.

Consistent with the results from the theoretical calculations, experimental results show that ELM amplitude and frequency can be varied by controlling access to the second ballooning stability regime at the edge through variation of the squareness of the discharge shape [9]. This is illustrated in Figs. 6 and 7 where the ELM frequency and amplitude as indicated by the divertor D_α radiation frequency and the change in edge T_e at various values of the squareness of the plasma shape are compared. As shown in Fig. 6, the plasma shape is rectangle-like at high squareness and triangle-like at low squareness. At low and high squareness the ELM frequency is strongly increased. The effects of the ELMs on the edge T_e are compared in Fig. 7. At high squareness, the ELM amplitudes are strongly reduced and there is no detectable change in the edge T_e. The ELM behavior at low squareness (not shown) is similar. The ballooning stability boundary of the high squareness discharge is also compared to that of the moderate squareness discharge in Fig. 7. At high squareness, access to the ballooning second stability regime is eliminated.

The results from the squareness experiments show that edge instabilities can be controlled by limiting the edge P' and J through elimination of the second ballooning stability access in the edge region. Motivated by these results, calculations have been carried out to evaluate the effects of a local perturbation of the plasma shape on the outboard bad curvature region on the ballooning stability. The results show that such a high order local perturbation of the plasma shape can also reduce and eliminate second ballooning stability access in the edge region. This is illustrated in Fig. 8. As the perturbation in the outboard region is increased, the second ballooning stability access is reduced and then eliminated. Since the perturbation is local, many of the favorable low n stability properties of Dee-shaped plasmas are also retained. Thus, localized shape perturbations may provide a means of obtaining plasmas with good overall β stability but with small benign ELMs. New experiments are being proposed in DIII–D to test the idea.
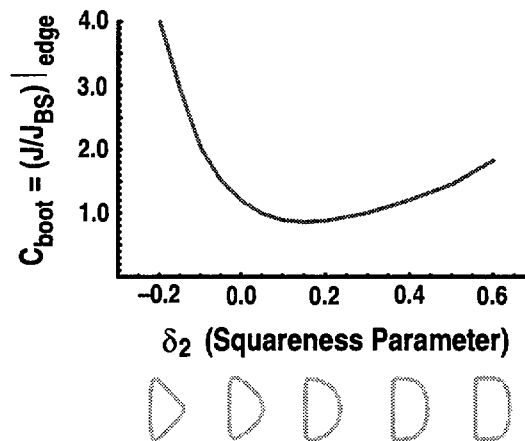

FIG. 5. Collisionless bootstrap current multiplier $C_{boot} = (J/J_{BS})/_{edge}$ required to gain second stability access in the plasma edge region varies with the squareness of the plasma shape, $R(\theta) = R_o + a\cos[\theta + \sin^{-1}(\delta\sin\theta)]$, $Z(\theta) = \kappa a \sin[\theta + \delta_2 \sin2\theta]$.
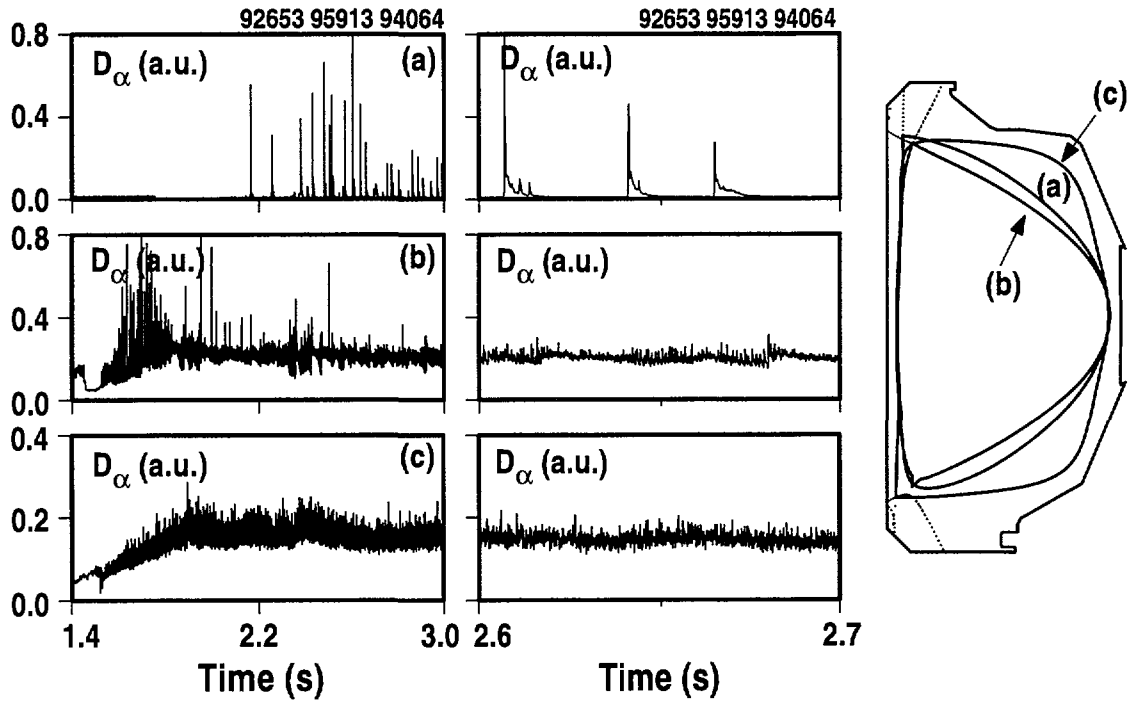
FIG. 6. Comparison of divertor D_α signals for 3 DIII–D discharges with (a) moderate squareness, (b) low squareness, and (c) high squareness.
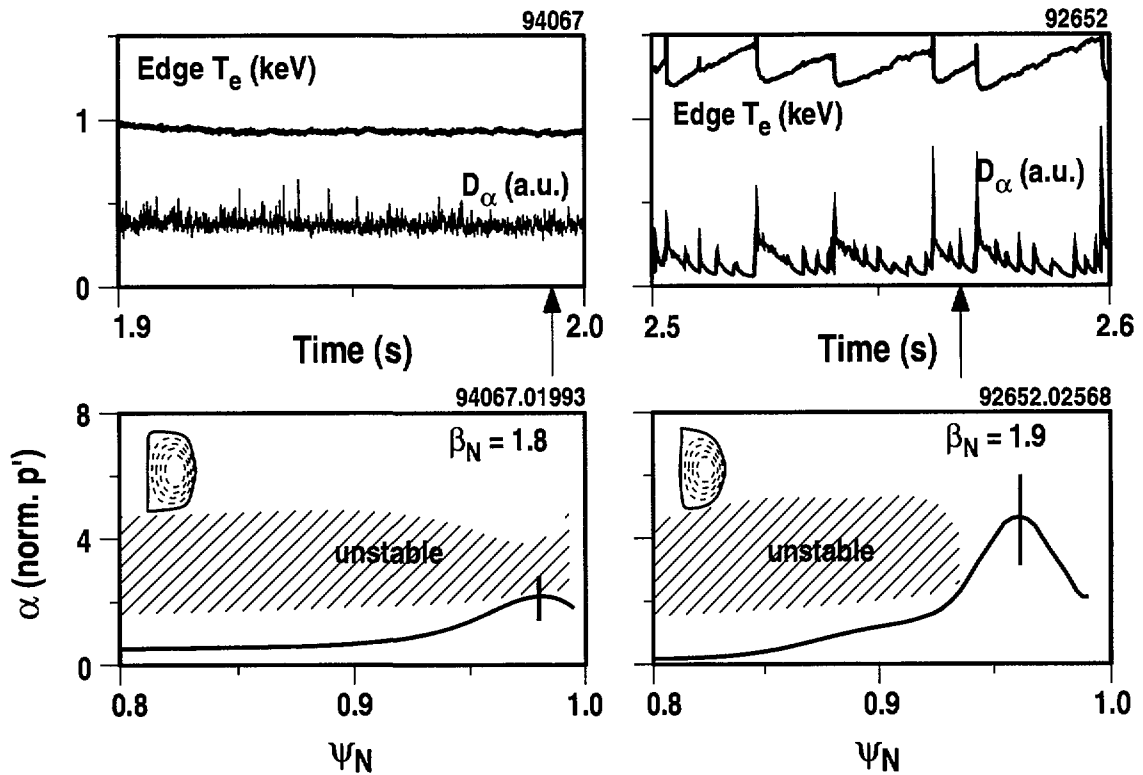

FIG. 7. Comparison of ideal ballooning stability, divertor D_α signals, and edge electron temperatures for a high squareness and a moderate squareness discharge. Arrows show time of stability calculations.
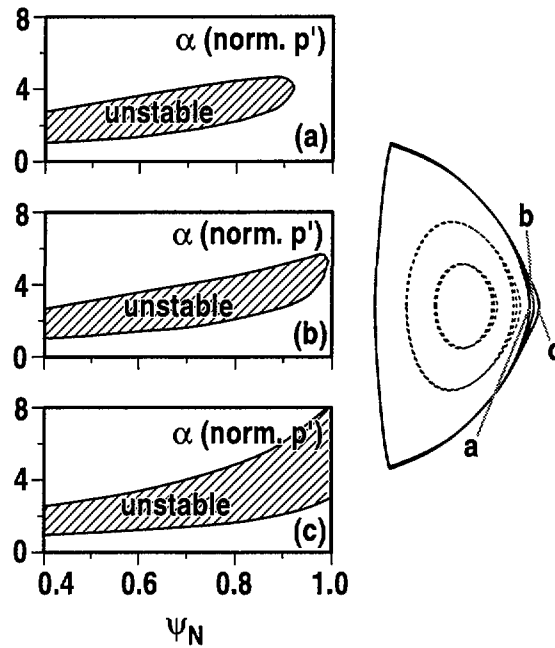
FIG. 8. Comparison of the ideal ballooning stability boundary for three simulated equilibria with (a) no perturbation of the plasma shape in the outboard bad curvature region, (b) moderate perturbation, and (c) large perturbation.

5. DISCUSSION AND SUMMARY

As shown in the previous sections, the performance of DIII–D H– and VH–mode discharges are limited by edge instabilities driven by the large edge P′ and J. Low to moderate n =2–9 magnetic precursors are often observed prior to the first giant type I ELM. Ideal stability analyses suggest that discharges with large edge P′ and J are more unstable to n > 1 modes as observed experimentally and that second ballooning stability access enhances the instabilities by facilitating the development of large edge P′ and J. The observed edge instabilities cannot be explained by a simple picture of instability to the high n ideal ballooning modes. Rather, the experimental and theoretical results suggest that they may be the outcome of a complex interaction among the high n ballooning modes, the intermediate to low n kink/ballooning/peeling modes, the edge P′, and the edge J. The results from the squareness experiments show that plasma shaping can provide an useful means to control edge instabilities.

ACKNOWLEDGEMENTS

REFERENCES

[1]   ZOHM, H., Plasma Phys. Control. Fusion 38, 105 (1996).
[2]   CONNOR, J.W., Plasma Phys. Control. Fusion 40, 531 (1998).
[3]   RICE, B.W., et al., Phys. Rev. Lett. 79, 2694 (1997).
[4]   OSBORNE, T.H., et al., in Controlled Fusion and Plasma Physics (Proc. 24th European Conf., Berchesgaden, 1997), Vol. 21A, Part III, EPS (1997) p. 1101.
[5]   STRAIT, E.J., et al., in Controlled Fusion and Plasma Physics (Proc. 20th European Conf., Lisbon, 1993), Vol. 17C, Part I, EPS (1993) p. 211.
[6]   FERRON, J.R., et al., in Controlled Fusion and Plasma Physics (Proc. 21st European Conf., Monpellier, 1994), Vol. 18B, Part I, EPS (1994) p. 86
[7]   LAO, L.L., et al., in Controlled Fusion and Plasma Physics (Proc. 24th European Conf., Berchesgaden, 1997), Vol. 21A, Part III, EPS (1997) p. 1117.

[8]   MILLER, R.L., *et al.*, Plasma Phys. Control. Fusion **40**, 753 (1998).

[9]   FERRON, J.R., *et al.*, GA-A22974 (1998), submitted to Nucl. Fusion.

[10] TURNBULL, A.D., *et al.*, GA-A22943 (1998), submitted to Phys. Plasmas.

[11] STRAIT, E.J., *et al.*, Phys. Plasmas **4**, 1783 (1997).

[12] TAYLOR, T.S., *et al.*, in Plasma Physics and Controlled Nuclear Fusion Research (Proc. 13th International Conf., Washington, D.C., 1990), IAEA, Vinenna, 1991, Vol. 1, p. 177.

[13] STRAIT, E.J., *et al.*, in Controlled Fusion and Plasma Physics (Proc. 18th European Conf., Berlin, 1991), Vol. 15C, Part II, EPS (1991) p. 105.

[14] HENDER, T.C., *et al.*, in Controlled Fusion and Plasma Physics (Proc. 24th European Conf., Berchesgaden, 1997), Vol. 21A, Part I, EPS (1997) p. 29.

[15] LAO, L.L., *et al.*, Nucl. Fusion **30**, 1035 (1990).

[16] MILLER, R.L., *et al.*, Phys. Plasmas **4**, 1062 (1997).

[17] BISHOP, C.M., *et al.*, Nucl. Fusion **24**, 1579 (1984).

[18] HUBBARD, A.E. , *et al.*, Phys. Plasmas **5**, 1744 (1998).

[19] BERNARD, L.C. , *et al.*, Comput. Phys. Commun. **24**, 377 (1981).

[20] HIRSHMAN, S.P., Phys. Fluids **31**, 3150 (1988).